Desalination and Water Treatment
www.deswater.com

doi: 10.5004/dwt.2022.27982

245 (2022) 202–216
January

Effect of metal cationic on the adsorption of selenium from sewage by biochar loaded with zero-valent iron

Chenao Lei[a], Baojun Yi[a,b,*], Weiqi Deng[a], Meijing Chen[a], Yuanyuan Wang[a,b]

[a]*College of Engineering, Huazhong Agricultural University, No. 1, Shizishan Street, Hongshan District, Wuhan 430070, China, Tel./Fax: +86 27 87282120; emails: bjyi@mail.hzau.edu.cn (B. Yi), lca@webmail.hzau.edu.cn (C. Lei), bjyi@mail.hzau.edu.cn (B. Yi), dengweiqi@webmail.hzau.edu.cn (W. Deng), 2017307220432@webmail.hzau.edu.cn (M. Chen), wangyuanyuan@mail.hzau.edu.cn (Y. Wang)*
[b]*Key Laboratory of Agricultural Equipment in the Mid-Lower Yangtze River, Ministry of Agriculture, Wuhan 430070, China*

Received 22 February 2021; Accepted 4 November 2021

ABSTRACT

The purpose of this study was to explore the feasibility of sawdust biochar loaded with zero-valent iron (SBC-nZVI) for the adsorption of Se(IV) in wastewater. The relationship between the adsorption of Se(IV) by SBC-nZVI and the dosage of SBC-nZVI, the concentration of Se(IV), the initial pH and final pH of Se(IV) solution, and the types and concentrations of ions in the solution were studied. The study found that the initial pH had little effect on the final removal rate, but had a greater impact on the adsorption rate; the pH of the solution after adsorption could be maintained between 3–3.5, which was beneficial to increase the adsorption rate; changing the ion concentration had little effect on adsorption, The ion type had a greater influence. There were both chemical adsorption and physical adsorption in the adsorption process. There were chemical adsorption and physical adsorption processes at the same time in the adsorption process. The high concentration of Ca^{2+} would hinder the membrane diffusion process, and the high concentration of Mg^{2+} would hinder the internal diffusion process, but the reaction rate did not significantly decrease under the experimental conditions. Experiments had proved that biochar loaded with nZVI could effectively adsorb Se(IV) in wastewater under various conditions, indicating that it was feasible to use SBC-nZVI for Se(IV) adsorption.

Keywords: SBC-nZVI; Adsorption; Se(IV); pH; Ion influence

1. Introduction

Selenium is an important trace element required by organisms and participates in many important physiological processes of organisms. Low concentration of selenium is beneficial to human health [1]. However, selenium is widely used in metallurgy, glass manufacturing, agriculture, chemical and other industries [2]. The discharge of wastewater causes the concentration of selenium in the water body to increase. The pollution of surface water and groundwater by high concentration selenium has become a global problem [3], it also threatens human health. The selenium element in nature exists in various valence states, and the specific forms are elemental selenium (Se^0), selenide (Se^{2-}), selenite(Se(IV)), and selenite (Se(VI)). According to the US EPA (FRL-5649-7) report, the acute toxicity of Se(IV) is almost 10 times that of Se(VI) [4]. Therefore, it is urgent to develop a treatment technology that effectively removes Se(IV).

A variety of methods can be used for the treatment of Se(IV) in wastewater, including chemical reduction, physical adsorption, membrane separation, flocculation and neutralization sedimentation, and biological treatment

* Corresponding author.

or a combination of multiple technologies [5]. Among them, zero-valent iron (nZVI) is widely used as a reducing agent for Se(IV) in wastewater due to its advantages of strong reducing ability, high efficiency of removing heavy metal pollutants, simple process and low operating cost. However, there are some obvious defects in the process of removing pollutants by nZVI: (i) Highly active nZVI is easily oxidized by air to form an oxide film, which hinders its contact with pollutants. (ii) Due to the high surface energy and intrinsic magnetic force, nZVI particles tend to aggregate into micron-level or larger particles, seriously reducing their reactivity [6]. To solve these problems, the researchers used a variety of materials to support nZVI particles, such as: bentonite, chitosan, kaolinite, mesoporous silica, etc. [7]. Compared with these materials, biochar has many obvious advantages. For example: (i) Biochar has a wide source, low cost, and is easy to recycle. (ii) Biochar has a large specific surface area and rich pore structure, which can disperse and stabilize nZVI particles [8], which is beneficial to reduce aggregation. (iii) Biochar itself is rich in functional groups and has a certain adsorption capacity for Se(IV) [9]. Previous studies have shown that biochar loaded with zero-valent iron (BC-nZVI) can effectively remove various pollutants in wastewater, including arsenate [10,11], selenate, selenite [12], Cr(VI) [13] and so on. Shang et al. [14] used herb residue biochar to load nZVI to remove Cr(VI) at a rate of up to 98.71%, and maintain its high efficiency in wastewater with high concentration of SO_4^{2-} and HA. Zhou et al. [15] found that by loading biochar onto nZVI, the composite material showed adsorption of heavy metals (Pb(II), Cr(VI) and As(V)), phosphate (P) and methylene blue (MB) ability enhancement. Therefore, the use of biochar loaded with zero-valent iron shows great potential for the removal of pollutants in the environment.

So far, nZVI removal of Se(IV) in wastewater has shown that pH is one of the most important factors affecting the removal efficiency. As the pH of the solution increases, the rate of nZVI removal of various pollutants in wastewater decreases [16,17]. When the pH is low, the enhanced reactivity of nZVI is caused by the acceleration of iron corrosion and the dissolution of the passivation film on the surface of nZVI, while at high pH, the reactivity of nZVI is reduced due to the formation of a precipitate, thereby inhibiting mass transfer [18]. Xia et al. [2] found that under acidic conditions, most of the nZVI is oxidized into Fe_3O_4 and amorphous FeOOH, while under alkaline conditions, the corrosion products are mainly $Fe(OH)_2$ and some Fe_3O_4. As can be seen from the above, pH may greatly affect the corrosion rate of nZVI and the conversion of iron (hydrogen) oxides. However, the nature of BC-nZVI and nZVI are very different. At present, there is a lack of research on the effect of pH on BC-nZVI. At the same time, due to the difference in the ratio of the adsorbent to the solution, whether the different pH conclusions are due to the change in the pH and acidity of the adsorbent. Therefore, the study of pH value has important guiding significance for the removal of Se(IV) in wastewater and the determination of the removal mechanism.

Similarly, various ions (including cations and inorganic anions) present in the wastewater may have an effect on the adsorption performance of nZVI. Dong et al. [19] tested the effect of some anions on the removal of selenate (Se(VI)) in water by zero-valent iron, and found that the inhibitory effect increased in the order of $Cl^- < NO_3^- < HCO_3^- < SO_4^{2-}$; in addition, nZVI removal Se(VI) also depends on the ion concentration. Previous studies have shown that SO_4^{2-} and PO_4^{2-} will increase the removal rate of Se(VI) by nZVI at low concentrations, and decrease the removal rate at high concentrations [20]. Anions may inhibit the interaction between nZVI and pollutants by competing for active sites with pollutants, and the effects of different kinds of ions may vary greatly. In general, the influence of cations is different from anions. Tan et al. [12] found that the presence of K^+, Ca^{2+}, and Mg^{2+} can enhance the ability of BC-nZVI to remove Se(IV) by reducing electrostatic repulsion. However, another study found that the presence of Ca^{2+} and Na^+ can cause the agglomeration of nZVI particles, which in turn reduces the removal rate of contaminants [21]. The impact of cations on the removal of pollutants by nZVI is somewhat controversial. In addition, compared with the research on the use of nZVI to remove selenium in water, the research is less on the removal of selenium by nZVI iron on biochar supported by cations in water, the mechanism of ions may be more complicated. Therefore, it is necessary to explore the effect of different concentrations of cations in the environment on the efficiency of BC-nZVI removal of Se(IV).

Therefore, based on the above analysis, the main objectives of this study are: (1). To study the effect of different initial and final pH values on the removal of Se(IV) by BC-nZVI. (2). Study the effect of different concentrations of Ca^{2+} and Mg^{2+} on the removal of Se(IV) by BC-nZVI. (3). According to the kinetic model, study the behavior characteristics of BC-nZVI to remove Se(IV).

2. Materials and method

2.1. Materials and preparation

Sawdust is sold online, washed with ultrapure water, dried in a constant temperature blast dryer (DHG-9243BS, Shanghai Xinmiao Medical Device Manufacturing Company), and then crushed with a crusher (Q-300B, Shanghai Bingdu Electric Co., Ltd.) Through a 60 mesh and 200 mesh sieve, take 200 to 60 mesh sawdust Sodium selenite (Na_2SeO_3), ferric chloride hexahydrate ($FeCl_3{\cdot}6H_2O$), anhydrous calcium chloride ($CaCl_2$), magnesium chloride hexahydrate ($MgCl_2{\cdot}6H_2O$), Chemical reagents such as potassium bromide KBr and hydrochloric acid (HCl) come from Sinopharm Group. All medicines are analytically pure, and the solution was prepared with ultrapure water.

In the experiment, pyrolysis method was used to prepare nZVI coated with biomass char. Weight 13.5150 g of ferric chloride hexahydrate dissolved in 800 mL of ultrapure water, stir to dissolve, then weight 20 g of wood chips into the solution to immerse and stir with a stirrer for 24 h. The mixture was placed in an oven at 105°C for 48 h and then taken out. It was crushed using an agate mortar to obtain Fe^{3+} impregnated sawdust. Finally, the sawdust impregnated Fe^{3+} were mixed evenly and placed in a tube furnace. The nitrogen gas was continuously fed and kept at a constant

temperature of 600°C for 2 h. The sample was naturally cooled to room temperature under continuous nitrogen gas flow. Sawdust biochar loaded with nano-zero-valent iron (SBC-nZVI) was obtained. The weighing results of several batches of SBC-nZVI indicate that the yield is 40%–50%.

2.2. Batch experiment operation

In the experiment, the wastewater environment was simulated concentrated, high-concentration ion wet power plant desulfurization wastewater, and sodium selenite was used as the typical form of Se. Weigh a certain amount of Na_2SeO_3 powder and dissolve in a certain amount of ultrapure water, and at the same time weigh a certain amount of metal salt in a small amount of ultrapure water, add to a volumetric flask to make a volume, use HCl to adjust the pH to a set value to obtain a sodium selenite solution that meets the experimental requirements. Weigh a certain amount of SBC-nZVI into a 50 mL centrifuge tube, add the pre-configured sodium selenite solution, and all the experiments in this paper were performed under shaking at a constant temperature of 25°C and 300 rpm. After a period of reaction, a sample was taken into a centrifuge for separation (TD25WS Changsha Xiangzhi Centrifuge Instrument Company), and the supernatant was taken to determine the total Se(IV) concentration. In order to ensure that the experimental conditions are basically the same, the sodium selenite solution used each time is newly prepared; before the experiment starts, the water bath shaker is turned on, adjusted to the set temperature, and then the sample and the solution are mixed. The removal efficiency (R (%)) and the adsorption capacity (q_e) of SBC-nZVI for Se(IV) are calculated according to the following formula:

$$q_t = \frac{(C_0 - C_t)V}{M} \tag{1}$$

$$\mathrm{Re} = \frac{(C_0 - C_e)}{C_0} \times 100\% \tag{2}$$

Among them, C_0, C_t and C_e are the initial concentration of the solution, the concentration at time t and the concentration of the solution at the time of adsorption equilibrium (mg/L), V is the solution volume (L), and M is the mass of the adsorbent added (g).

In order to explore the influence of different Se(IV) concentrations on the adsorption experiment, 3 g/L SBC-nZVI was added into plastic bottles containing 50 mL of Se(IV) solution with initial concentration of 10, 20, 30, 40 and 50 mg/L, respectively. The shaking adsorption was carried out at 300 rpm and 25°C. After 2 h, took a sample and centrifuge and took the supernatant to determine the remaining Se(IV) in the solution to determine the best adsorbent dosage. In order to explore the effect of different adsorbent dosages on the adsorption experiment, the initial dosages of SBC-nZVI of 1, 2, 3, 4 and 5 g/L were added in a plastic bottle with a 50 mL Se(IV) solution (40 mg/L, unadjusted pH), shake and adsorb at 300 rpm and 25°C. Sample and centrifuge at regular intervals and take the supernatant to measure the residual Se(IV) in the solution. In order to explore the effect of the initial pH of different solutions on the adsorption of Se(IV), the pH of the selenium solution with Se(IV) concentration of 40 mg/L was adjusted to 4, 5, 6, and 7 using hydrochloric acid, respectively. Then add 3 g/L of SBC-nZVI to a plastic bottle containing 50 mL of Se(IV) solution (40 mg/L), shake and adsorbed at 300 rpm, 25°C, sample and centrifuge at regular intervals and take the supernatant to measure the remaining Se(IV) in the solution to determine the optimal initial pH of the solution. In order to explore the effect of different concentrations and different types of cations on the adsorption of Se(IV), the concentrations of Ca^{2+} and Mg^{2+} in the experiment were adjusted to 2,000; 4,000 and 6,000 mg/L using anhydrous $CaCl_2$, $MgCl_2{\cdot}6H_2O$, respectively. And set up a group of control groups without adding Ca^{2+} and Mg^{2+}, respectively. The Se(IV) concentration of the selenium solution is 40 mg/L, and the pH is adjusted to 6 using hydrochloric acid. Add 3 g/L of SBC-nZVI to a plastic bottle containing 50 mL of Se(IV) solution (40 mg/L, pH = 6), shake and adsorb at 300 rpm, 25°C, and sample and centrifuge at regular intervals And take the supernatant to measure the remaining Se(IV) in the solution.

2.3. Analytical method

In the study, a Fourier infrared spectrometer (Nicolet iS50 Thermo Fisher Scientific) was used to analyze the surface functional groups of the SBC-nZVI samples before and after the reaction. The sample is made by tableting method. Before preparation, the SBC-nZVI samples before and after the reaction and the KBr as the background were ground and crushed in an agate mortar, and then fully dried in an oven at 100°C. Take 5 mg of sample and KBr in a ratio of 1:80, and then place it on the tablet press to maintain the pressure of 20 MPa for 30 s, and finally get a tablet sample. In the study, an atomic absorption spectrophotometer (AA-6880F/AAC Shimadzu Instruments (Suzhou) Co., Ltd.) was used to determine the concentration of Se(IV) in the solution. The test method is the flame method, which used acetylene and air to burn to produce a flame. The acetylene flow rate is 3.7 L/min, the lamp current is 23 mA, the wavelength is 196.0 nm, the burner height is 15 mm, and the slit width is 0.5 nm. The as adsorbed SBC-nZVI at 25°C, 40 mg/L Se(IV), pH = 6, with additional addition of 4,000 mg/L Ca^{2+} and Mg^{2+} were collected and denoted as SBC-nZVI-Se, SBC-nZVI-Se/Ca with SBC-nZVI-Se/Mg, respectively. Another small amount of SBC-nZVI as received sample, which was quickly rinsed with deionized water, filtered and oven dried at 105°C along with the three chars, was used to perform the char properties tests.

2.4. Adsorption isotherm

The following four isotherm models were fitted and analyzed for the process of Se(IV) adsorption by SBC-nZVI:

Langmuir isotherm:

$$\frac{C_e}{q_e} = \frac{1}{K_L q_m} + \frac{C_e}{q_m} \tag{3}$$

Freundlich isotherm:

$$\ln q_e = \ln K_F + \frac{1}{n} C_e \tag{4}$$

Temkin isotherm:

$$q_e = \frac{RT}{b_T} \ln K_T + \frac{RT}{b_T} \ln C_e \tag{5}$$

D–R adsorption isotherm equation:

$$\ln q_e = \ln q_m - \beta\varepsilon^2 \tag{6}$$

$$\varepsilon = RT \ln\left(1 + \frac{1}{C_e}\right) \tag{7}$$

$$E_a = \frac{1}{\sqrt{2\beta}} \tag{8}$$

where q_m (mg/g) is the maximum adsorption amount, C_e (mg/L) is the equilibrium concentration, q_e (mg/g) is the equilibrium adsorption amount of the adsorbate, K_L (L/mg) is the Langmuir bonding term related to the interaction energies, K_F (L/mg) is the Freundlich model affinity coefficient and n is the Freundlich linear constant. K_T (L/mg) is the adsorption equilibrium constant, B_T is the Temkin constant, and R_T/B_T (J/mol) is related to the heat of adsorption, β (mol²/kJ²) and ε are the Dubinin–Radushkevich (D–R) isotherm constants.

2.5. Adsorption thermodynamics

The thermodynamic parameters of the reaction were calculated to explore its thermodynamic characteristics using the following equation:

$$\Delta G° = -RT \ln\left(K_e^0\right) \tag{9}$$

$$\ln\left(K_e^0\right) = \frac{\Delta S°}{R} - \frac{\Delta H°}{RT} \tag{10}$$

$$K_e^0 = \frac{\text{1,000 kg molecular weight of adsorbate} \left[\text{adsorbate}\right]^0}{\gamma} \tag{11}$$

where T is kelvin temperature (K), R is the gas constant (8.314 J/mol K), and K_e^0 is the thermodynamic equilibrium constant calculated from Eq. (9) [23]. γ is the coefficient of activity, [adsorbate]⁰ is the standard concentration of adsorbate (1 mol/L), and K_g is the K in the best fit isotherm model. $\Delta G°$ is calculated from Eq. (7), and the $\Delta H°$ and $\Delta S°$ can be calculated by plotting the $\ln K_e^0$ and $1/T$ as the figure showed.

2.6. Adsorption kinetics

The experimental conditions of adsorption kinetics were the same as the experimental conditions above. The pseudo-first order and (PFO) the pseudo-second order (PSO) were used to fit them respectively. According to the fitting degree R^2, the equation with good fitting degree could be regarded as the kinetic equation for Se(IV) removal by SBC-nZVI. The intra-particle diffusion (IPD) and film diffusion (FD) were also used to fit the data to determine the changes in the reaction stage.

Pseudo-first order:

$$\log\left(q_e - q_t\right) = \log q_e - \frac{K_f}{2.303} t \tag{12}$$

Pseudo-second order:

$$\frac{t}{q_t} = \frac{1}{K_s q_e^2} - \frac{1}{q_e} t \tag{13}$$

Intra-particle diffusion:

$$q_t = K_i t^{1/2} + c_i \tag{14}$$

Film diffusion:

$$F = 1 - \left(\frac{6}{\pi^2}\right) \exp\left(-B_t\right) \tag{15}$$

Among them, q_e (mg/g) and q_t (mg/g) are the adsorption amount of adsorbent to Se(IV) at adsorption equilibrium and adsorption time t; K_f (min⁻¹), K_s (g/(mg min)) and K_i (mg/(g min$^{0.5}$)) represent pseudo-first order and pseudo-second order parameters; c_i is the intercept related to the boundary layer; F is the fraction of equilibrium adsorption capacity at time t and B_t is a mathematical function of F.

Eq. (13) can be deformed as:

$$B_t = -0.4977 - \ln\left(1 - F\right) \tag{16}$$

F is calculated as:

$$F = \frac{q_t}{q_e} \tag{17}$$

3. Results and discussions

3.1. Effect of selenium concentration on adsorption characteristic

It can be seen from Fig. 1 that the dosage of 3 g/L has a higher adsorption rate for solutions with Se(IV) concentrations of 10–50 mg/L, of which the removal rate of 40 mg/L highest. When the concentration of Se(IV) is less than 40 mg/L, the removal rate increases with the increase of selenium concentration, which is inconsistent with the experimental results of Lv et al. [22]. After the reaction, the final Se(IV) concentration of the diluted solutions of

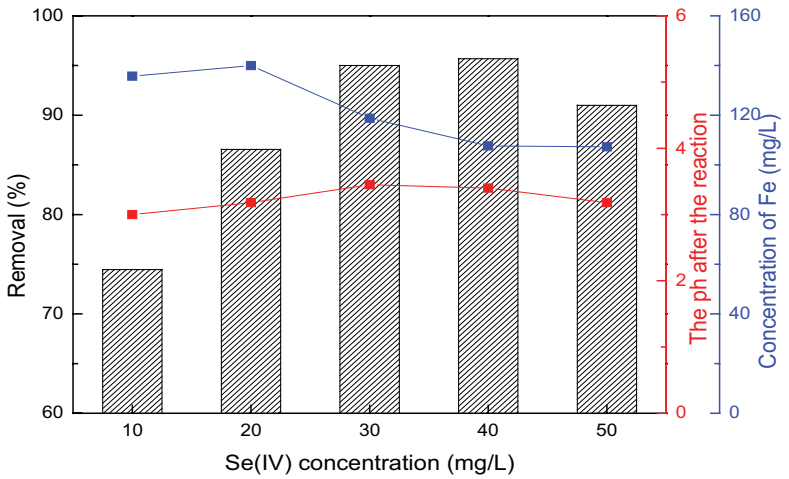

Fig. 1. Effects of SBC on the removal rate and solution characteristics of Se(IV) in Se(IV) solution.

various concentrations was measured to be 1.5–3 mg/L. It is speculated that the Se(IV) concentration may be reduced to a concentration where SBC-nZVI cannot work at 2 h, and the initial concentration increased, calculated by the formula, which showed the removal rate continues to increase. For a 50 mg/L Se(IV) solution, the removal rate decreased at this concentration. This was because as the concentration of Se(IV) in the solution increases, the competition between Se(IV) increases, and the dosage of SBC-nZVI is constant, and the reactive sites on the surface are limited, resulting in a decrease in the final removal rate. Previous studies showed that the main mechanism of nZVI removal of Se(IV) [23,24].

$$2Fe^0 + SeO_3^{2-} + 6H^+ \rightarrow 2Fe^{2+} + Se^0 \downarrow + 3H_2O \quad (18)$$

The generated Fe^{2+} may continue to react with the corresponding oxidizing pollutants to be further oxidized to Fe^{3+} [25]. Since Na_2SeO_3 itself is alkaline, as the concentration of Se(IV) increases, the pH of the solution increases, and part of Fe^{3+} forms a precipitate, resulting in a decrease in the concentration of Fe^{3+}. In general, due to the consumption of H^+ in the solution, the pH of the solution should increase. However, after the nZVI reaction was supported by biochar in this experiment, the pH of solution was maintained at 3–3.5, which may be caused by the hydrolysis of Fe^{3+} and Fe^{2+}. Importantly, lower pH is very advantageous for nZVI to remove Se(IV). Previous studies found that lower pH would reduce the thickness of the oxide layer on the surface of nZVI and promote the release of Fe^{2+} [2]. The resulting Fe^{2+} adsorbed on the surface of nZVI or was released into the solution. The Fe(II) ions absorbed in the surface structure increase the electrical conductivity of the surface oxide layer and reduce the electron transfer barrier on the corroded coating, thereby significantly enhancing the electron transfer [26], and thus promoting Se(IV)-Fe^0 reaction. Xu et al. [27] found that Fe(II) dissolved in solution played an important role in activating nZVI as the main electron donor for reducing Se(IV), indicating that more Fe^{2+} produced under acidic conditions was helpful to the removal of Se(IV) by SBC-nZVI. In addition, the corrosion products formed under acidic conditions are Fe_3O_4 and amorphous FeOOH [2]. These corrosion products could not only act as intermediates for electron transfer, but also provided more reaction/adsorption sites for Se(IV) adsorption and reduction. Therefore, the acidic environment formed by biochar loaded with nZVI had a very important role in promoting the removal of Se(IV).

3.2. Effect of adsorption parameters on the adsorption effect of Se(IV) in solution

As can be seen from Fig. 2a, when the amount of adsorbent was less than 3 g/L, the removal efficiency increased significantly with the increase of adsorbent. According to previous reports, the mechanism of biochar loaded with zero-valent iron to remove Se(IV) in water mainly includes reduction, adsorption and co-precipitation [28]. The increase of SBC-nZVI provides more active sites for Se(IV) attachment. The enhanced adsorption of biochar and the reduction of zero-valent iron results in a faster removal rate of Se(IV). When the amount of SBC-nZVI was further increased, the removal rate of Se(IV) did not continue to increase or even slightly decreased. This is because the accumulation of biochar restricted the exposure of surface sites, resulting in the removal efficiency no longer increasing. Therefore, according to the removal rate and removal efficiency shown in the figure, the dosage of subsequent experiments was set to 3 g/L.

It can be seen from Fig. 2b that when the pH is less than 7, the final removal rate of Se(IV) is equal for all groups when they are in equilibrium, reaching more than 90%, which indicates that SBC-nZVI is used to remove Se(IV) from wastewater great potential. Before reaching equilibrium, as the pH increases, the reaction rate decreases, which is consistent with previous conclusions [2,17]. According to Eq. (6), the pH is lowered, the promotion effect of the reaction is enhanced, the rate of reduction of Se(IV) by Fe^0 is accelerated, and the Fe^{2+} generated at the same time is increased, and the presence of Fe^{2+} can enhance the

electron transport ability [27], which promote the reduction of Se(IV). In addition, due to the higher H^+ concentration, the reduction potential of Fe/Fe^{2+} increases, resulting in higher activity of nZVI particles [29]. In addition, the increased pH may cause the formation of ferrous hydroxide and precipitate on the surface of nZVI, blocking the reaction site, thus reducing the overall reaction rate [21]. However, it was interesting that the final removal rate of Se(IV) at different pH was comparable, possibly due to the removal of Se(IV) by biochar through adsorption, thereby reducing the difference in removal rate of Se(IV) at different pH [12]. According to previous reports, the pK_{a1} and pK_{a2} of H_2SeO_3 are 2.62 and 8.23, respectively, so when the pH was less than 8, the main form of selenium was $HSeO_3^-$. Since the pH range of the entire experiment (4–7) was less than the pH_{pzc} of biochar, the surface of biochar was positively charged. There was a strong electrostatic attraction between positively charged biochar and negatively charged $HSeO_3^-$, resulting in a high adsorption capacity when the pH was less than 7. Considering that the desulfurization wastewater was mostly weakly acidic, the pH of the selenium solution was adjusted to 6 in subsequent experiments on cations.

3.3. Effect of cation in sewage on Se(IV) adsorption in solution

It can be seen from Fig. 3a that the Ca^{2+} set in the experiment had not much effect on the removal of Se(IV) in water by SBC-nZVI. The removal rate was basically the same in the first period of time, and the final removal rate of the reaction might be slightly reduced only in the late period of the reaction, indicating that the presence of Ca^{2+} had a certain inhibitory effect on the removal of Se(IV) in water by SBC-nZVI. Studies had shown that the presence of Ca^{2+} can lead to the agglomeration of nZVI particles [30,31] or occupy active sites on nZVI surface [21]. Compared with previous studies [22,32,33], the inhibitory effect of Ca^{2+} on SBC-nZVI in this experiment was negligible. This was due to biochar loading, which could reduce this aggregation. At the same time, biochar is positively charged in this environment, and electrostatic repulsion with Ca^{2+} prevents Ca^{2+} from occupying the active site of nZVI, resulting in insignificant reduction in removal efficiency. It can be seen that SBC-nZVI-Se/Ca overcomes the interference of Ca^{2+} and ensures the normal progress of the reaction.

It can be seen from Fig. 3b that the rate of removal of Se(IV) is highest in the group of samples without Mg^{2+}

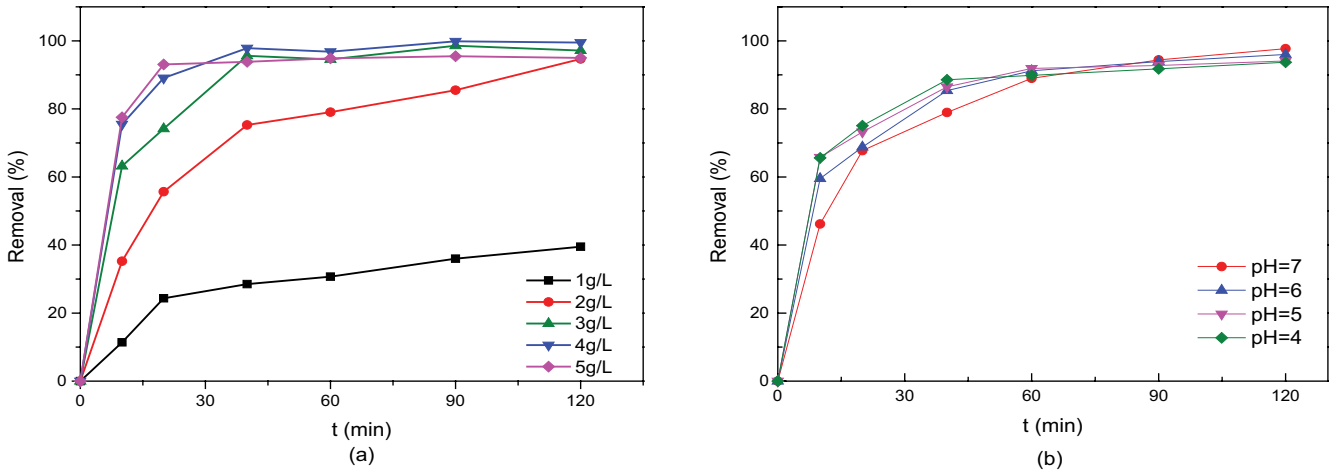

Fig. 2. The effect of initial adsorption parameters on the removal rate of Se(IV) in solution: (a) Adsorbent dosage and (b) pH.

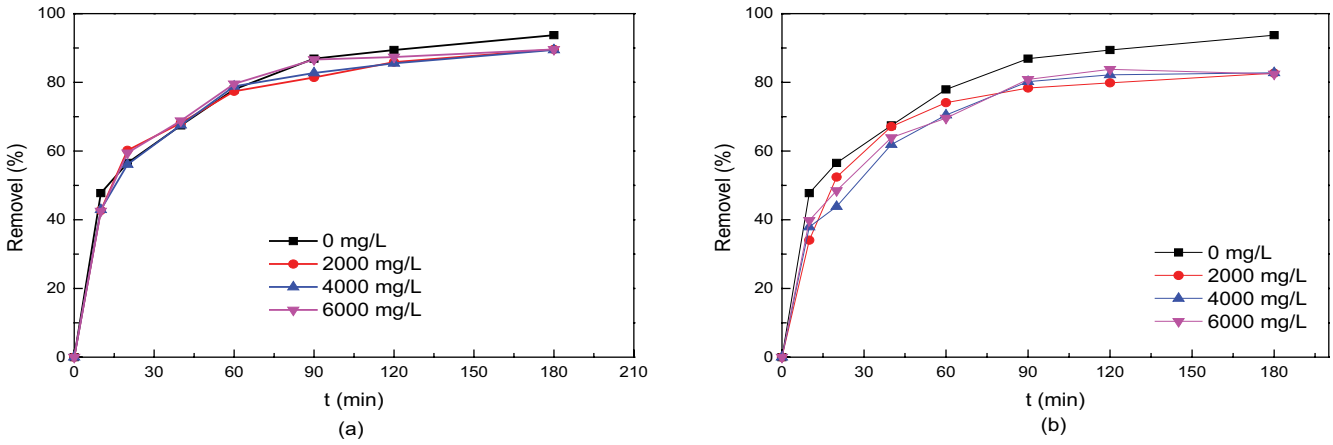

Fig. 3. The effect of cations in the solution on the removal of Se(IV): (a) Ca^{2+} and (b) Mg^{2+}.

addition, while the removal rate of the three groups of Mg^{2+} added are decreased. Therefore, it can be considered that Mg^{2+} generally has an inhibitory effect on the removal of Se(IV) from SBC-nZVI in water. This may be due to Mg^{2+} competing for the binding site of SBC-nZVI [22]. Compared with other experiments, the removal rate under the action of Mg^{2+} in this experiment was only reduced by about 10%, which is far less than the inhibitory effect of Mg^{2+} in other experiments [32,34]. Therefore, it can be concluded that the loading of biochar can alleviate the inhibitory effect of Mg^{2+} on nZVI. Compared with the previous set of experiments, it can be seen that the inhibition effect of Mg^{2+} is more obvious than that of Ca^{2+} with the same concentration. This may be because Mg^{2+} in aqueous solution is easier to precipitate as hydroxide than Ca^{2+}, and the hydroxide coated on the surface of nZVI greatly limits its reactivity [34]. It is worth noting that as the Ca^{2+} and Mg^{2+} concentrations continue to increase, the final removal rate of Se(IV) remains basically unchanged. The results show that Se(IV) and SBC-nZVI may form an inner complex, which is less affected by ionic strength [35,36].

3.4. Surface analysis

3.4.1. Surface functional group groups analysis

In order to explore the changes of SBC-nZVI functional groups, FTIR was tested and shown in Fig. 4. There were several obvious characteristic peaks, located at 666; 896; 1,396; 1,645; 1,718; 2,905 and 3,479 cm^{-1} respectively. The characteristic peaks near 666 and 896 cm^{-1} showed C–H out-of-plane bending, and SBC-nZVI-Se vibration was the weakest. Characteristic peaks near 1,396 cm^{-1} showed in-plane bending of –OH. The characteristic peak near 1,645 cm^{-1} showed stretching of C=C. The peak near 1,718 cm^{-1} represented the presence of C=O. The characteristic peak near 2,905 cm^{-1} was caused by C–H stretching, and the vibration was weak. The characteristic peak near 3,479 cm^{-1} was caused by –NH stretching, which demonstrated the presence of amino functional groups in SBC-nZVI. Therefore, it could be concluded that some changes in surface functional groups occurred before and after SBC-nZVI adsorbed Se(IV) and other substances. Meanwhile, a large number of oxygen-containing functional groups on the surface of SBC-nZVI provided active sites for Se(IV) removal.

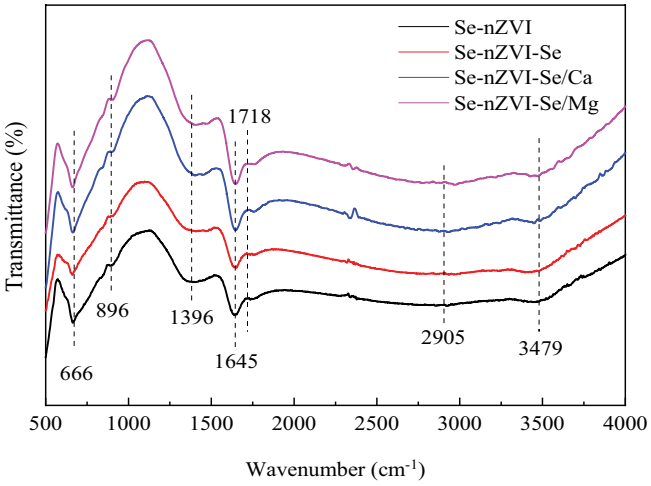

Fig. 4. FTIR spectra of SBC from rice straw or wood chips before and after the reaction.

3.4.2. XPS analysis

The XPS test results are shown in Figs. 5 and 6. From Fig. 5, the peak of Fe^0 decreased from 20.30% to 8.61%, Fe^{2+} increased from 15.44% to 27.57%, and Fe^{3+} slightly decreased from 64.25% to 63.81% after adsorption Se in the condition of without interfering ions. It showed that the reaction described in Eq. (16) did take place in the experiment. Fe^0 was oxidized to Fe^{2+} first, and then further oxidized to Fe^{3+}. In the same time, Fe^0 on the surface of SBC-nZVI with Ca^{2+} and Mg^{2+} disappeared, and all the elemental iron was oxidized. Fe^{2+} increased to 28.23% and 20.70%, and the proportion of Fe^{3+} increased to 71.77% and 79.30%, respectively, indicating that the added ions increased the rate of oxidation reaction. Fig. 6 shows that Se(0) (55.38–55.74 eV) and Se(IV) (58.45–58.71 eV) mainly existed on the surface of adsorbent after reaction, indicating that direct adsorption and reduction processes of Se(IV) existed in the reaction. The SBC-nZVI-Se scan showed that Se(0) and Se(IV) accounted for 46.56% and 53.44%, respectively, indicating that the contribution rates of physical adsorption and chemical reduction were almost equal. After Ca^{2+} existence, the adsorption capacity of Se(IV) on SBC-nZVI decreased, and the ratio of Se(0) and Se(IV) on the surface was 60.06% and 39.94%, respectively. However, no obvious peak value was detected by scanning Ca2p, indicating that Ca^{2+} were not deposited on the surface of SBC-nZVI-Se/Ca. It indicated that Ca^{2+} may hinder the diffusion process of adsorbed surface film, but did not affect the overall reaction rate. The Se3d images of SBC-nZVI-Se/Mg and SBC-nZVI showed little difference (Se(0) and Se(IV) accounted for 47.09% and 52.91% respectively), but the peak value of Mg^{2+} (1304.13 eV) appeared in the scanning of Mg1s, indicating the presence of Mg^{2+} on the surface. However, the removal of Se(IV) was not hindered.

3.4.3. BET specific surface area test

BET test results are shown in Table 1. In terms of specific surface area, SBC-nZVI had a large specific surface area and a small pore size, forming more micropores and mesopores. As the adsorption progressed, the pore size, pore volume and specific surface area of SBC-nZVI-Se increased. Presumably, the reason was that the adsorbed Se was deposited on SBC-nZVI. When Ca^{2+} existed in Se(IV) solution, it had little effect on Se(IV) adsorption. When Mg^{2+} was present in the Se(IV) solution, the attachment of Mg^{2+} on the surface of SBC-nZVI caused a rapid decrease in specific surface area and pore volume.

3.5. Analysis of adsorption mechanism

3.5.1. Adsorption isotherms

According to the data in Table 2 and Fig. 7, it can be seen that the first three models had good fitting degree.

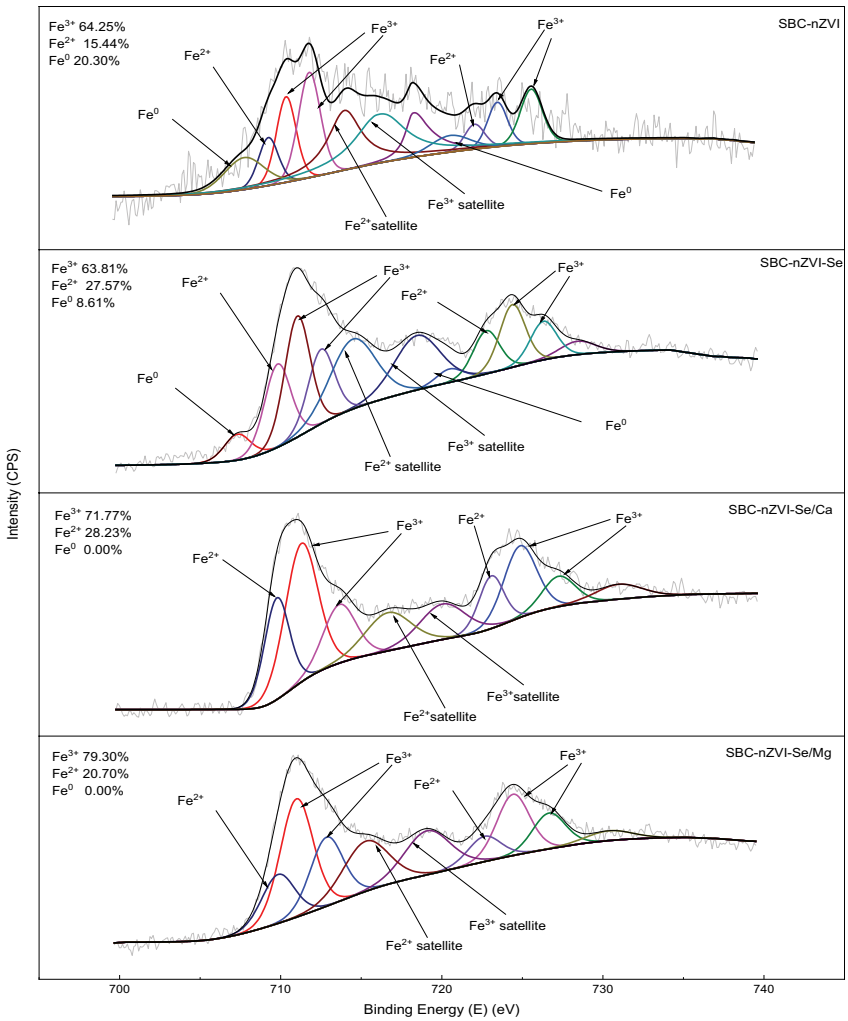

Fig. 5. XPS spectra and analysis of Fe2p.

Among all models, the Freundlich fitting degree (R^2) was the highest, indicating that SBC-nZVI conforms to the description of the isothermal equation, indicating that the surface of SBC-nZVI was not uniform and there was multilayer adsorption. Langmuir adsorption model was the next best, and the equation showed that monolayer adsorption accounted for a certain proportion of the reaction. Temkin's model was different from the previous two models in that it assumed that the adsorption energy decreased linearly due to surface coverage, which was more suitable for explaining the chemisorption process, and the described chemisorption process was generally regarded as electrostatic interaction [37].

For Langmuir equation, the degree of difficulty of adsorption reaction can be determined according to the shape of isotherm [38]. $R_L = 1/(1 + C_0K_L)$ was defined as an invariant factor to indicate the advantage of adsorption, where C_0 was the initial concentration of dye solution, when $0 < R_L < 1$ was the advantage of adsorption, $R_L > 1$ was adverse adsorption, $R_L = 0$ was irreversible adsorption, and $R_L = 1$ was linear adsorption [39]. In this experiment, $0 < R_L = 0.163107, 0.144433, 0.111057 < 1$, indicating that it was favorable for adsorption. For Freundlich equation, $1/n = 0.5, 0.494, 0.442 < 1$, indicating that the adsorption process was easy to occur.

3.5.2. Adsorption thermodynamic and analysis

Thermodynamic analysis results are shown in Table 3. Where $0 << \Delta H° < 20$ kJ/mol indicated that physical adsorption was involved in the adsorption process, and $\Delta G° < 0$ also indicated that the reaction can be spontaneous.

The analysis of isotherm model and thermodynamic data showed that the maximum adsorption capacity q_m did not change much under the influence of temperature, indicating that the adsorption of Se(IV) by SBC-nZVI might involve a physical process. Meanwhile, Freundlich model had a high degree of fitting, which indicated that Se removal was related to physical adsorption. Langmuir model and Temkin model could fit the experimental data well, indicating that the adsorption process conformed to the hypothesis of the equation and was related to the chemical mechanism, which was consistent with the result of kinetic analysis. In addition, BET tests showed that there were

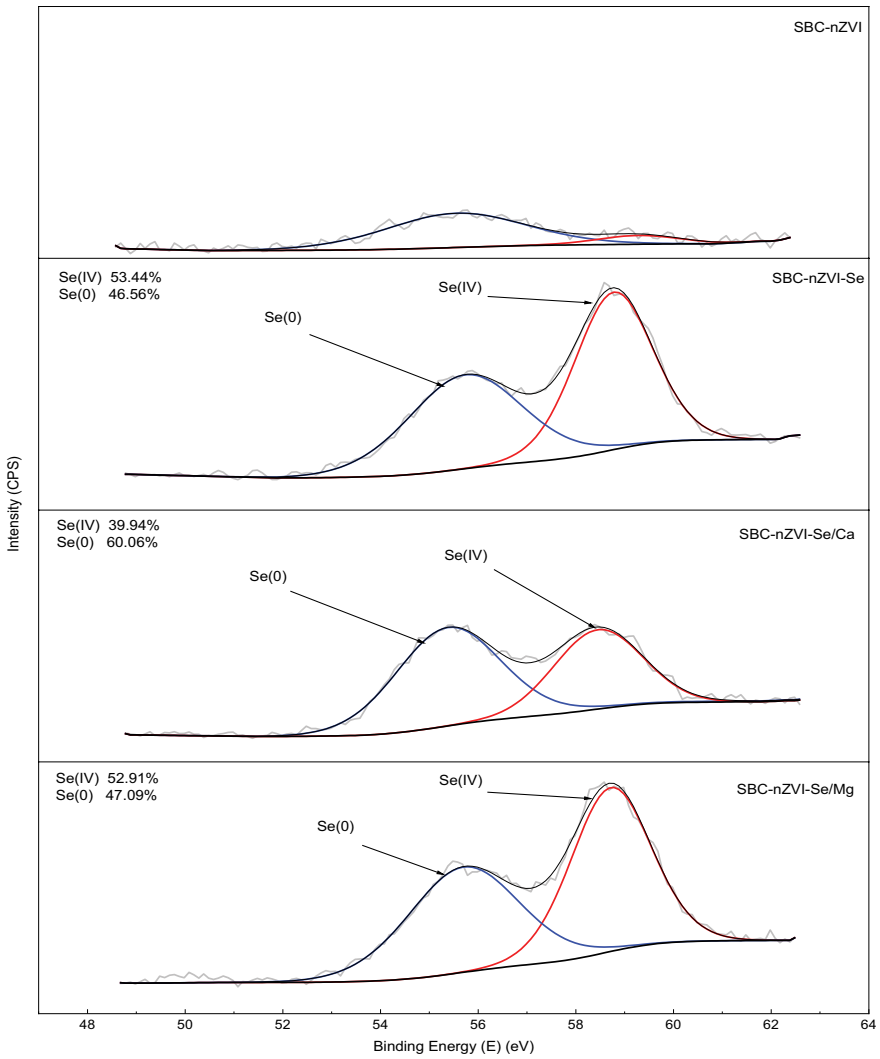

Fig. 6. XPS spectra and analysis of Se3d.

Table 1
BET surface test

Characteristics	Sample			
	SBC-nZVI	SBC-nZVI-Se	SBC-nZVI-Se/Ca	SBC-nZVI-Se/Mg
Surface area (m^2/g)	332.638	342.261	341.314	288.039
Pore volume (cm^3/g)	0.159	0.169	0.170	0.144
Pore size (nm)	7.219	9.819	11.758	12.838

monolayer and multilayer adsorption phenomena when SBC-nZVI adsorbed Se(IV), suggesting that physical and chemical adsorption existed in the process simultaneously.

3.5.3. The adsorption kinetics

The kinetic analysis was used PFO. The fitting calculation results are shown in Table 4.

As can be seen from Table 4, under the experimental conditions, in all experiments, the measurement coefficient R^2 (0.9779–0.9999) of the PSO was higher than that of the PFO (0.5417–0.9927). Compared with the PFO, the q_e value calculated using the PSO was closer to the experimental data. Therefore, the PSO could better describe the adsorption behavior of Se(IV) on SBC-nZVI. According to previous studies, the kinetics of iron-loaded granular activated carbon for the removal of selenite in wastewater was also better suited to the PSO [40]. It showed that the removal of Se(IV) by SBC-nZVI was mainly controlled by the chemical adsorption mechanism. It could be seen from Fig. 8a and

Table 4 that the higher the SBC-nZVI dosage, the higher the K_2 value of the fitted line, indicating that its removal rate was accelerating; but the adsorption capacity of selenium per unit adsorbent decreased due to the unsaturated surface active sites of the adsorbent. In contrast, combining the image in Fig. 8b and the data in the pH section of Table 4, it could be seen that a lower pH had a certain increase in the removal rate, but the effect was not obvious. Comparing the values of Ca^{2+} and Mg^{2+} in Figs. 8c, 8d and Table 4, it could be seen that high concentration of Mg^{2+} reduces the reaction rate and the final adsorption rate, while high concentration of Ca^{2+} had little effect on the reaction.

Fig. 9 is the fitted image of the IPD under all conditions in the experiment. The curve was linear but did not pass the origin, indicating that the IPD was not the only rate. control step. According to Onal et al. [41], the nonlinearity of the IPD curve indicated that the adsorption process has multiple adsorption stages. The first stage was a rapid FD process, followed by a slower IPD process, during which Se(IV) was reduced or adsorbed on the surface or inner

Table 2
Adsorption isotherm parameters

Model		T (K)		
		288.15	298.15	308.15
Langmuir	q_m	17.085	17.409	17.141
	k_L	0.128	0.148	0.2
	R^2	0.955	0.961	0.905
Freundlich	K_F	2.956	3.264	4.076
	$1/n$	0.5	0.494	0.442
	R^2	0.977	0.967	0.918
Temkin	b_T	593.087	600.361	669.358
	k_T	1.068	1.224	1.917
	R^2	0.959	0.963	0.877
D–R	q_m	10.916	11.41	11.158
	β	2.030×10^{-6}	1.600×10^{-6}	7.290×10^{-7}
	E_a	496.04	559.017	828.18
	R^2	0.879	0.906	0.699

Table 3
Adsorption thermodynamic parameters

T (K)	K_F (L/mg)	K_e^0	$\Delta G°$ (kJ/mol)	$\Delta H°$ (kJ/mol)	$\Delta S°$ (J/mol K)
288.15	2.956452	12.36068667	–31.507		
298.15	3.263891	12.45961667	–32.845	11.783	150.017
308.15	4.075608	12.68171667	–34.515		

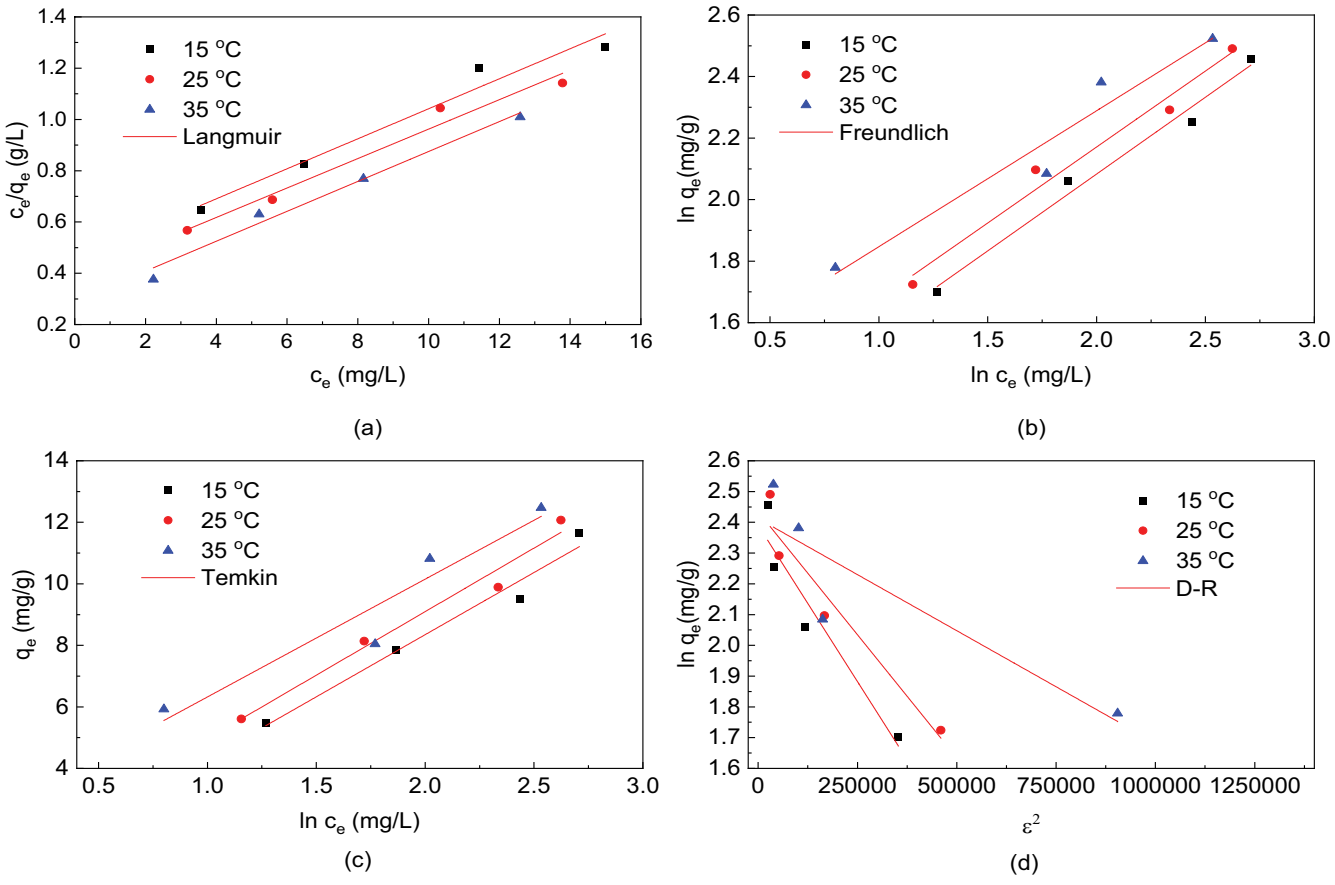

Fig. 7. Isothermal adsorption: (a) SBC-nZVI, (b) SBC-nZVI-Se, (c) SBC-nZVI-Se/Ca, and (d) SBC-nZVI-Se/Ca.

Table 4
Reaction kinetic analysis of each group of experiments

Variable		Pseudo-first-order			Pseudo-second-order		
		q_e (min/(mg/g))	K_1	R^2	q_e (min/(mg/g))	K_2	R^2
SBC-nZVI (g/L)	1	8.569	–0.02073	0.7548	14.52	0.002613	0.9779
	2	9.745	–0.02169	0.9262	17.02	0.002845	0.9941
	3	5.365	–0.05373	0.6968	10.75	0.01564	0.9983
	4	5.678	–0.09067	0.9191	7.958	0.04131	0.9997
	5	0.8106	–0.05110	0.5417	5.984	0.1115	0.9997
pH	7	7.893	–0.03351	0.9918	12.84	0.005856	0.9994
	6	6.084	–0.03685	0.9890	12.17	0.009897	0.9995
	5	5.495	–0.05117	0.8054	11.88	0.01554	0.9984
	4	3.274	–0.03171	0.9029	11.48	0.01968	0.9998
Ca^{2+} (mg/L)	0	8.062	–0.02236	0.9907	13.86	0.004536	0.9975
	2,000	6.931	–0.02163	0.9814	13.09	0.005518	0.9990
	4,000	7.139	–0.02259	0.9773	13.14	0.005336	0.9993
	6,000	7.864	–0.02784	0.9927	13.19	0.005752	0.9994
Mg^{2+} (mg/L)	0	8.062	–0.02236	0.9907	13.86	0.004536	0.9975
	2,000	4.915	–0.02434	0.9536	12.49	0.01009	0.9999
	4,000	9.165	–0.03931	0.9656	12.68	0.008002	0.9989
	6,000	8.529	–0.04141	0.8887	12.62	0.009085	0.9981

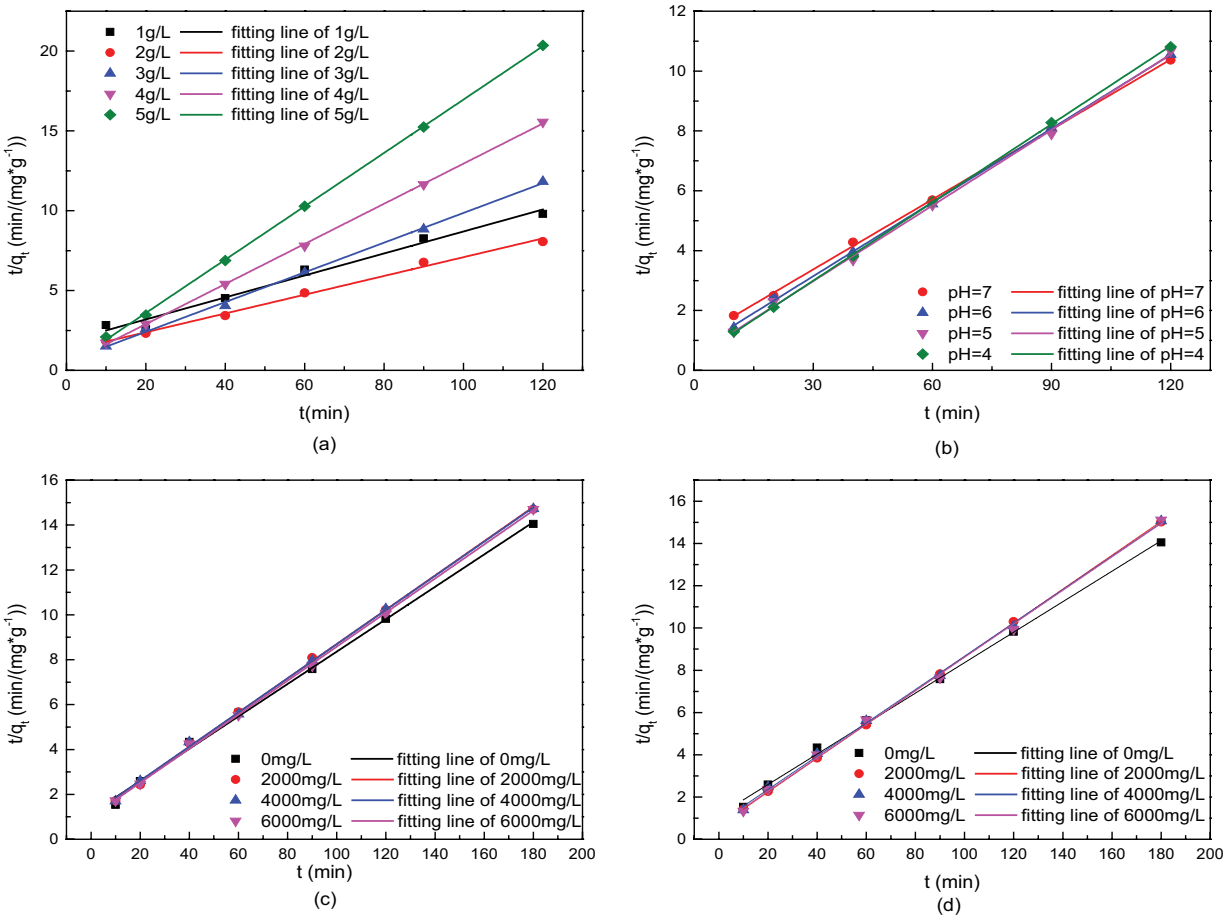

Fig. 8. Pseudo-second-order (PSO) fitting image. (a) The addition amount of SBC-nZVI, (b) pH, (c) Ca^{2+}, and (d) Mg^{2+}.

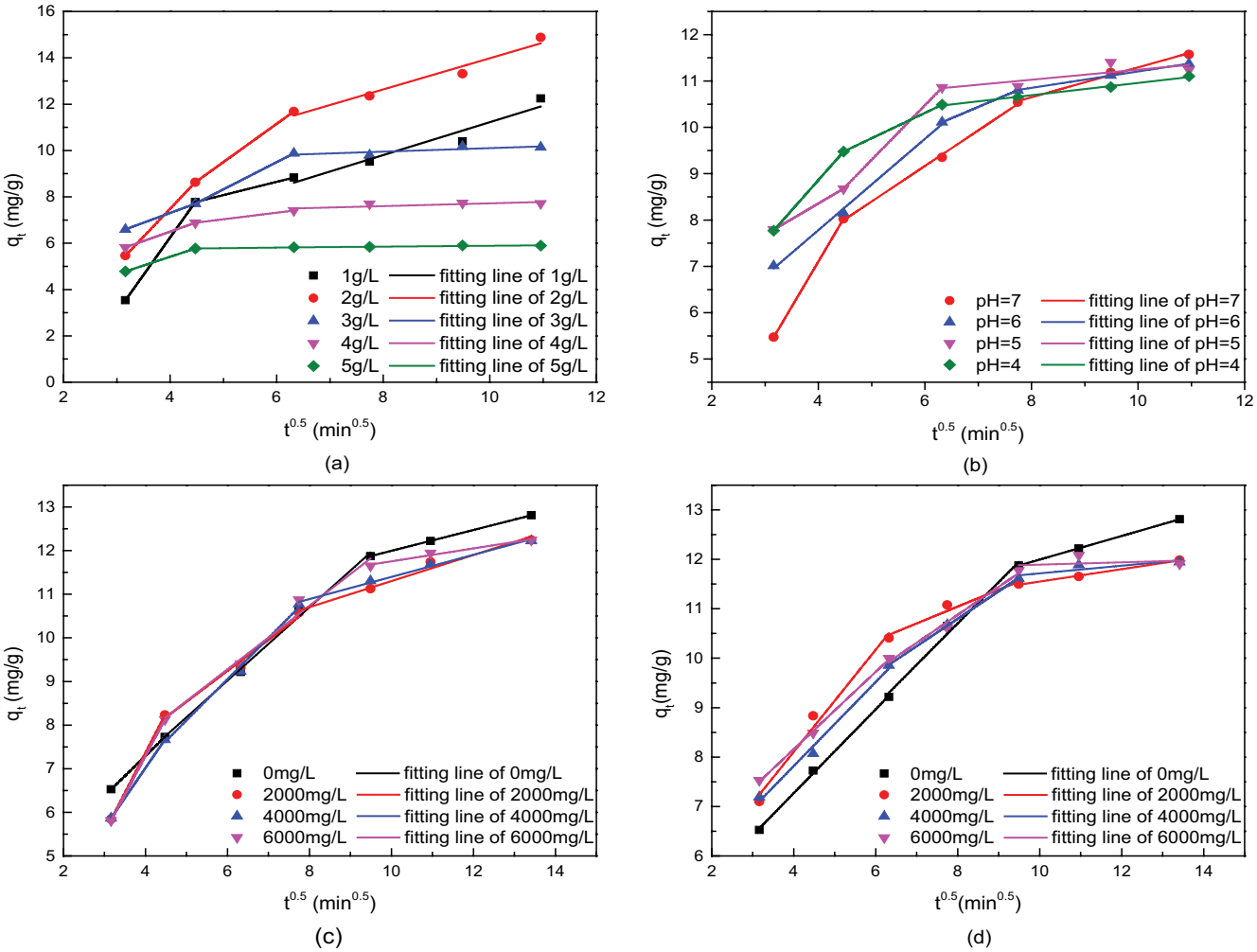

Fig. 9. The intraparticle diffusion (IPD) fitting image. (a) The addition amount of SBC-nZVI, (b) pH, (c) Ca^{2+}, and (d) Mg^{2+}.

surface, and finally the IPD process gradually reached equilibrium (the third stage).

The curve is multi-linear for the removal process of Se(IV). In the process of adsorbing solid/liquid adsorption, the transport of adsorption is usually the diffusion of the liquid phase to the outer surface of the adsorbent (membrane diffusion) and the absorption of the adsorbate into the internal pores of the adsorbent (internal diffusion), or both. Multiple linearity means that Se(IV) consists of three stages (except 5 g/L), and the order of rate constant is K_1 (the first stage) > K_2 (the second stage) > K_3 (the third stage). This means that the first stage is a rapid membrane diffusion process, followed by a slower internal diffusion process, during which Se(IV) is reduced or adsorbed on the surface or inner surface, and finally the internal diffusion gradually reaches equilibrium (the three stages). With the increase of the dosage, the third stage line diagram of the dosage of 3 g/L and above began to appear almost parallel, indicating that the dosage of SBC-nZVI here and above can already deal with 40 mg/L more thoroughly of selenium solution. This is also the reason why the dosage of 3 g/L was used in the previous experiment. In addition, for the two groups with SBC-nZVI dosages of 4 and 5 g/L, the boundaries between the second and third stages became blurred, and the fitting lines of the two stages nearly overlapped. It is speculated that With the increase of the dosage, the Se(IV) per unit area treatment is less, the membrane diffusion rate was lower (unsaturated), and the reactants entering the second stage were reduced, so that the internal diffusion process was no longer the part that limited the overall reaction rate. It could be seen from Fig. 6b that the reaction rate of each stage of the four groups accelerated with the decrease of pH, indicating that the acidic environment was conducive to the rapid removal of Se(IV) in water by SBC-nZVI.

Figs. 9c and d were the fitting images of the IPD of the experiment to study the effects of Ca^{2+} and Mg^{2+}, respectively. It could be seen from the figure that these two reactions were also divided into the three stages described above. For Ca^{2+} (Fig. 9c), the mass transfer effect of the reaction was slightly affected and slightly reduced. XPS analysis showed that Ca^{2+} might occupy the active adsorption site in FD stage and hindered the adsorption from FD stage to IPD stage. However, due to the slow IPD process, the final adsorption effect was not significantly affected. The high concentration of Mg^{2+} ions affected the final IPD process to some extent, which was consistent with the BET test results.

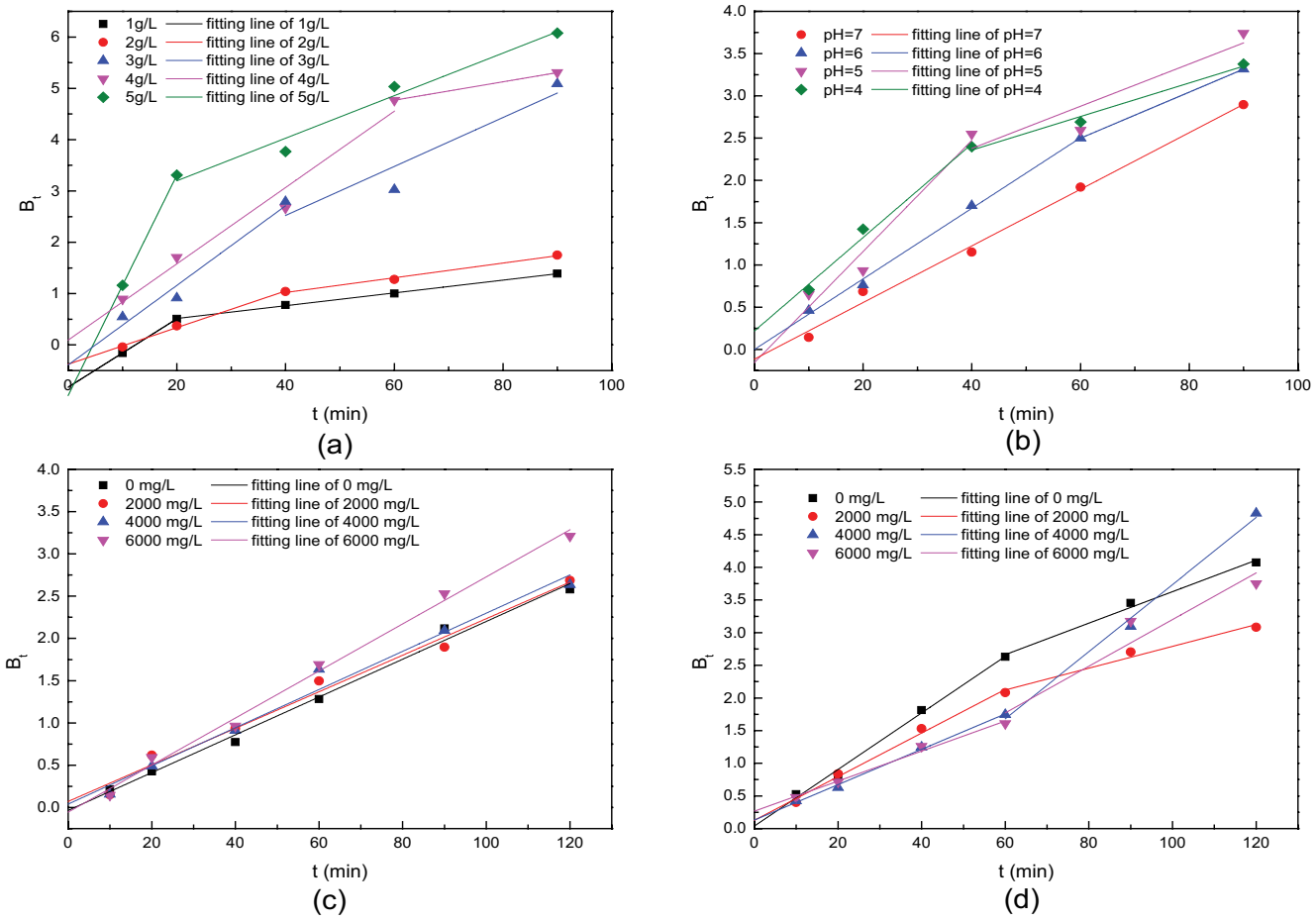

Fig. 10. The film diffusion (FD) model fitting image. (a) The addition amount of SBC-nZVI, (b) pH, (c) Ca^{2+}, and (d) Mg^{2+}.

However, due to the excellent adsorption performance of SBC-nZVI, the final adsorption effect did not change much.

Considering the film diffusion process, the mechanism were also were fitted by FD model, and the results are shown in Fig. 10. When the fitted line was a straight line and past the origin, it indicated that the adsorption rate was subject to intra particle diffusion, otherwise the membrane diffusion was the rate limiting step [42]. It could be seen that the fitting line in the case of Ca^{2+} addition was to go as a straight line through the origin, and the remaining several sets of reactions basically consisted of two stages, but the first stage fitting line also basically passed through the origin or close to the origin, indicating that membrane diffusion hardly became the rate limiting step of this reaction. For different loadings, either too high or too low amounts shifted the fitted line of the first phase away from the origin, indicating that membrane diffusion was the rate limiting step at this time, presumably as too high dosing caused the Se(IV) concentration to drop rapidly and the reactions occurring on the membrane layer to decrease rapidly when conditioned by reactants for very short periods of time; The large deviation of the fitted line from the origin at pH = 4 for different pH presumably resulted from the competition between H^+ and Se(IV) in the acidic environment, making membrane diffusion the rate limiting step. For the two groups with cations added, the fitted line almost concentrated through the origin, indicating that membrane diffusion was not the rate limiting step, the appeared hindered phenomenon in adsorption occurred in the inner diffusion phase, which is consistent with the previous conclusion.

4. Conclusions

A zero-valent iron adsorbent loaded with sawdust biochar was prepared and used in the adsorption experiment of Se(IV). The results show that SBC-nZVI has a strong adsorption performance for Se(IV) in a wide pH range, which enables SBC-nZVI to effectively remove Se(IV) under various conditions. During the reaction, a lower pH was formed in the solution, which significantly promoted the removal of Se(IV) by SBC-nZVI. Appropriate dosage and a weakly acidic environment are conducive to the rapid occurrence of the membrane diffusion reaction of SBC-nZVI adsorbing Se(IV) and accelerating the reaction. The process of SBC-nZVI adsorbing Se(IV) had both physical and chemical adsorption processes, which was a complex process of interaction between two adsorption methods. High concentration of Ca^{2+} and low concentration of Mg^{2+} would accelerate the oxidation of elemental iron, and high concentration of Ca^{2+} would affect the membrane diffusion step, high concentration of Mg^{2+} would be deposited on SBC-nZVI, Affect the internal diffusion process, but under the

test conditions, the two ions would not significantly reduce the Se(IV) removal efficiency of SBC-nZVI. Therefore, SBC-nZVI had the potential to be a good adsorbent for removing Se(IV) from aqueous solutions.

Acknowledgments

This work was supported by the Fundamental Research Funds for the Central Universities (2662019PY018, 202010504053), the Major Projects of Technical Innovation of Hubei Province (2019ACA153), and the Natural Science Foundation of Hubei Provincial (2017CFB231). The authors also acknowledge the extended help from the Analytical and Testing Center of Huazhong Agricultural University (HZAU).

References

[1] H.K. Hansen, S.F. Peña, C. Gutiérrez, A. Lazo, P. Lazo, L.M. Ottosen, Selenium removal from petroleum refinery wastewater using an electrocoagulation technique, J. Hazard. Mater., 364 (2019) 78–81.
[2] X. Xia, L. Ling, W.-x. Zhang, Solution and surface chemistry of the Se(IV)-Fe(0) reactions: effect of initial solution pH, Chemosphere, 168 (2017) 1597–1603.
[3] S.-H. Hong, F.N. Lyonga, J.-K. Kang, E.-J. Seo, C.-G. Lee, S. Jeong, S.-G. Hong, S.-J. Park, Synthesis of Fe-impregnated biochar from food waste for Selenium(VI) removal from aqueous solution through adsorption: process optimization and assessment, Chemosphere, 252 (2020) 126475.
[4] R. López de Arroyabe Loyo, S.I. Nikitenko, A.C. Scheinost, M. Simonoff, Immobilization of selenite on Fe_3O_4 and Fe/Fe_3C ultrasmall particles, Environ. Sci. Technol., 42 (2008) 2451–2456.
[5] P. Cordoba, L.C. Staicu, Flue gas desulfurization effluents: an unexploited selenium resource, Fuel, 223 (2018) 268–276.
[6] J. Wang, W. Zhang, X. Kang, C. Zhang, Rapid and efficient recovery of silver with nanoscale zerovalent iron supported on high performance activated carbon derived from straw biomass, Environ. Pollut., 255 (2019) 113043.
[7] H. Dong, J. Deng, Y. Xie, C. Zhang, Z. Jiang, Y. Cheng, K. Hou, G. Zeng, Stabilization of nanoscale zero-valent iron (nZVI) with modified biochar for Cr(VI) removal from aqueous solution, J. Hazard. Mater., 332 (2017) 79–86.
[8] H. Su, Z. Fang, P.E. Tsang, J. Fang, D. Zhao, Stabilisation of nanoscale zero-valent iron with biochar for enhanced transport and in-situ remediation of hexavalent chromium in soil, Environ. Pollut., 214 (2016) 94–100.
[9] J.S. Clemente, S. Beauchemin, T. MacKinnon, J. Martin, C.T. Johnston, B. Joern, Initial biochar properties related to the removal of As, Se, Pb, Cd, Cu, Ni, and Zn from an acidic suspension, Chemosphere, 170 (2017) 216–224.
[10] S. Wang, B. Gao, Y. Li, A.E. Creamer, F. He, Adsorptive removal of arsenate from aqueous solutions by biochar supported zero-valent iron nanocomposite: batch and continuous flow tests, J. Hazard. Mater., 322 (2017) 172–181.
[11] H. Zhu, Y. Jia, X. Wu, H. Wang, Removal of arsenic from water by supported nano zero-valent iron on activated carbon, J. Hazard. Mater., 172 (2009) 1591–1596.
[12] G. Tan, Y. Mao, H. Wang, M. Junaid, N. Xu, Comparison of biochar- and activated carbon-supported zerovalent iron for the removal of Se(IV) and Se(VI): influence of pH, ionic strength, and natural organic matter, Environ. Sci. Pollut. Res. Int., 26 (2019) 21609–21618.
[13] L. Wu, L. Liao, G. Lv, F. Qin, Y. He, X. Wang, Micro-electrolysis of Cr(VI) in the nanoscale zero-valent iron loaded activated carbon, J. Hazard. Mater., 254–255 (2013) 277–283.
[14] J. Shang, M. Zong, Y. Yu, X. Kong, Q. Du, Q. Liao, Removal of chromium (VI) from water using nanoscale zerovalent iron particles supported on herb-residue biochar, J. Environ. Manage., 197 (2017) 331–337.
[15] Y. Zhou, B. Gao, A.R. Zimmerman, H. Chen, M. Zhang, X. Cao, Biochar-supported zerovalent iron for removal of various contaminants from aqueous solutions, Bioresour. Technol., 152 (2014) 538–542.
[16] S. Wang, Y. Song, Y. Sun, Enhanced dyes removal by sulfidated zerovalent iron: Kinetics and influencing factors, Envirion. Technol. Innovation, 11 (2018) 339–347.
[17] L. Liang, W. Yang, X. Guan, J. Li, Z. Xu, J. Wu, Y. Huang, X. Zhang, Kinetics and mechanisms of pH-dependent selenite removal by zero valent iron, Water Res., 47 (2013) 5846–5855.
[18] S. Bae, K. Hanna, Reactivity of nanoscale zero-valent iron in unbuffered systems: effect of pH and Fe(II) dissolution, Environ. Sci. Technol., 49 (2015) 10536–10543.
[19] H. Dong, Y. Chen, G. Sheng, J. Li, J. Cao, Z. Li, Y. Li, The roles of a pillared bentonite on enhancing Se(VI) removal by ZVI and the influence of co-existing solutes in groundwater, J. Hazard. Mater., 304 (2016) 306–312.
[20] J. Qiao, Y. Song, Y. Sun, X. Guan, Effect of solution chemistry on the reactivity and electron selectivity of zerovalent iron toward Se(VI) removal, Chem. Eng. J., 353 (2018) 246–253.
[21] K. Lin, J. Ding, X. Huang, Debromination of tetrabromobisphenol A by nanoscale zerovalent iron: kinetics, influencing factors, and pathways, Ind. Eng. Chem. Res., 51 (2012) 8378–8385.
[22] D. Lv, X. Zhou, J. Zhou, Y. Liu, Y. Li, K. Yang, Z. Lou, S.A. Baig, D. Wu, X. Xu, Design and characterization of sulfide-modified nanoscale zerovalent iron for cadmium(II) removal from aqueous solutions, Appl. Surf. Sci., 442 (2018) 114–123.
[23] T. Chen, L. Luo, S. Deng, G. Shi, S. Zhang, Y. Zhang, O. Deng, L. Wang, J. Zhang, L. Wei, Sorption of tetracycline on H_3PO_4 modified biochar derived from rice straw and swine manure, Bioresour. Technol., 267 (2018) 431–437.
[24] L. Liang, X. Guan, Z. Shi, J. Li, Y. Wu, P.G. Tratnyek, Coupled effects of aging and weak magnetic fields on sequestration of selenite by zero-valent iron, Environ. Sci. Technol., 48 (2014) 6326–6334.
[25] R.M. Powell, R.W. Puls, S.K. Hightower, D.A. Sabatini, Coupled iron corrosion and chromate reduction: mechanisms for subsurface remediation, Environ. Sci. Technol., 29 (1995) 1913–1922.
[26] J.A. Mielczarski, G.M. Atenas, E. Mielczarski, Role of iron surface oxidation layers in decomposition of azo-dye water pollutants in weak acidic solutions, Appl. Catal., B, 56 (2005) 289–303.
[27] L. Xu, Y. Huang, Kinetics and mechanism of selenite reduction by zero valent iron under anaerobic condition activated and enhanced by dissolved Fe(II), Sci. Total Environ., 664 (2019) 698–706.
[28] L. Ling, B. Pan, W.-x. Zhang, Removal of selenium from water with nanoscale zero-valent iron: mechanisms of intraparticle reduction of Se(IV), Water Res., 71 (2015) 274–281.
[29] L. Huang, S. Zhou, F. Jin, J. Huang, N. Bao, Characterization and mechanism analysis of activated carbon fiber felt-stabilized nanoscale zero-valent iron for the removal of Cr(VI) from aqueous solution, Colloids Surf., A, 447 (2014) 59–66.
[30] F. He, D. Zhao, Manipulating the size and dispersibility of zerovalent iron nanoparticles by use of carboxymethyl cellulose stabilizers, Environ. Sci. Technol., 41 (2007) 6216–6221.
[31] J. Gao, L. Yang, Y. Liu, F. Shao, Q. Liao, J. Shang, Scavenging of Cr(VI) from aqueous solutions by sulfide-modified nanoscale zero-valent iron supported by biochar, J. Taiwan Inst. Chem. Eng., 91 (2018) 449–456.
[32] D. Li, X. Zhu, Y. Zhong, W. Huang, P. a. Peng, Abiotic transformation of hexabromocyclododecane by sulfidated nanoscale zerovalent iron: kinetics, mechanism and influencing factors, Water Res., 121 (2017) 140–149.
[33] C. Shen, W. Lu, Y. Huang, J. Wu, H. Zhang, Removal of bismerthiazol from water using zerovalent iron: Batch studies and mechanism interpretation, Chem. Eng. J., 260 (2015) 411–418.
[34] H. Lu, C. Wen, S. Gao, Y. Dong, M. Zhang, B. Li, W. Hu, J. Dong, Incorporation of nanoscale zero-valent iron particles in monodisperse mesoporous silica nanospheres:

characterization, reactivity, transport in porous media, Colloids Surf., A, 553 (2018) 28–34.
[35] L.E. Katz, L.J. Criscenti, C.-c. Chen, J.P. Larentzos, H.M. Liljestrand, Temperature effects on alkaline earth metal ions adsorption on gibbsite: approaches from macroscopic sorption experiments and molecular dynamics simulations, J. Colloid Interface Sci., 399 (2013) 68–76.
[36] N. Sleiman, V. Deluchat, M. Wazne, M. Mallet, A. Courtin-Nomade, V. Kazpard, M. Baudu, Phosphate removal from aqueous solutions using zero valent iron (ZVI): influence of solution composition and ZVI aging, Colloids Surf., A, 514 (2017) 1–10.
[37] F. Kallel, F. Chaari, F. Bouaziz, F. Bettaieb, R. Ghorbel, S.E. Chaabouni, Sorption and desorption characteristics for the removal of a toxic dye, methylene blue from aqueous solution by a low cost agricultural by-product, J. Mol. Liq., 219 (2016) 279–288.
[38] G. Crini, P.-M. Badot, Application of chitosan, a natural aminopolysaccharide, for dye removal from aqueous solutions by adsorption processes using batch studies: a review of recent literature, Prog. Polymer Sci., 33 (2008) 399–447.
[39] L. Liu, Y. Lin, Y. Liu, H. Zhu, Q. He, Removal of methylene blue from aqueous solutions by sewage sludge based granular activated carbon: adsorption equilibrium, kinetics, and thermodynamics, J. Chem. Eng. Data, 58 (2013) 2248–2253.
[40] N. Zhang, L.-S. Lin, D. Gang, Adsorptive selenite removal from water using iron-coated GAC adsorbents, Water Res., 42 (2008) 3809–3816.
[41] Y. Onal, C. Akmil-Basar, C. Sarici-Ozdemir, Investigation kinetics mechanisms of adsorption malachite green onto activated carbon, J. Hazard. Mater., 146 (2007) 194–203.
[42] T. Mahmood, S.U. Din, A. Naeem, S. Tasleem, A. Alum, S. Mustafa, Kinetics, equilibrium and thermodynamics studies of arsenate adsorption from aqueous solutions onto iron hydroxide, J. Ind. Eng. Chem., 20 (2014) 3234–3242.